

Causal Balancing for Domain Generalization

Xinyi Wang¹, Michael Saxon¹, Jiachen Li¹, Hongyang Zhang², Kun Zhang³,
William Yang Wang¹

¹Department of Computer Science, University of California, Santa Barbara, USA

²David R. Cheriton School of Computer Science, University of Waterloo, Canada

³Department of Philosophy, Carnegie Mellon University, USA

xinyi_wang@ucsb.edu, saxon@ucsb.edu, jiachen_li@ucsb.edu,
hongyang.zhang@uwaterloo.ca, kunz1@cmu.edu, william@cs.ucsb.edu

Abstract

While machine learning models rapidly advance the state-of-the-art on various real-world tasks, out-of-domain (OOD) generalization remains a challenging problem given the vulnerability of these models to spurious correlations. We propose a causally-motivated balanced mini-batch sampling strategy to transform the observed train distribution to a balanced distribution that is free of spurious correlations. We argue that the Bayes optimal classifiers trained on such balanced distribution is minimax optimal across a diverse enough environment space. We also provide an identifiability guarantee of the latent variable model of the proposed underlying data generation process with invariant causal mechanisms, by utilizing enough number of train environments. Experiments are conducted on three domain generalization datasets, demonstrating empirically that our balanced mini-batch sampling strategy improves the performance of four different established domain generalization model baselines compared to the random mini-batch sampling strategy.

1 Introduction

Machine learning is achieving tremendous success in many fields with useful real-world applications [1–3]. While machine learning models can perform well on in-domain test data with the same distribution as their training data, they often fail to generalize to out-of-domain (OOD) data sampled from unseen environments [4, 5]. One explanation for such a failure is that the models are prone to learning spurious correlations that change between environments. For example, in image classification tasks, instead of relying on the object of interest, machine learning models easily rely on surface-level textures [6, 7] or background environments [8, 9] that are unstable when the image style changes or when the image is in a novel background environment. This vulnerability to changes in environments can cause serious problems for machine learning systems deployed in real-world scenarios, calling into question their reliability over time. Thus, approaches that can provide guarantees to model robustness under shifting environment-driven spurious correlations between input features and target labels are desirable. An increasingly popular way to achieve this is by leveraging causal modeling.

Many classification tasks aim to learn an inverse mapping of an underlying causal mechanism through which data is generated. For example, in object recognition, the identity of the depicted object (and thus the image label Y) drives its appearance (a subset of features in the image X); the task of identifying Y from X thus can be considered as modeling the inverse of this causal process [10]. Methods that can reliably capture these domain-invariant causal features and disregard domain-variant spuriously correlated ones are thus less susceptible to performance degradation due to changes in the spuriously correlated feature distribution under domain shifts [11]. Such methods often aim to find invariant data representations using new loss function designs that incorporate the invariance



(a) Observed distribution $p(X, Y|E = e)$

(b) Balanced distribution $\hat{p}(X, Y|E = e)$

Figure 1: The causal graphical model assumed for data generation process in environment $e \in \mathcal{E}$. Shaded nodes means being observed and white nodes means not being observed. Black arrows means causal relations invariant across different environments. Red dashed line means correlation varies across different environments.

conditions across different domains into the training process. Representative examples include the invariance of linear classifiers on top of data representations [12], the invariance of causal/semantic features [13–15], and the invariance of calibration [16]. Unfortunately, these approaches have to contend with trade-offs between weak simple models or approaches without theoretical guarantees [12, 16], and empirical studies have shown their utility in the real world to be questionable [17].

An ideal approach to domain shift vulnerability mitigation would identify spurious confounders automatically by analyzing the data distribution, be simple enough to support useful theoretical guarantees, and deliver empirical performance gains. In this paper, we present progress toward this goal by decomposing domain-variant spurious correlation mitigation into two steps: first learning the observed data distribution using *Latent Covariate Learning*, and then using these representations to create a *balanced mini-batch sampling* strategy that is balanced with respect to the spurious correlations, to ensure the domain-invariant causal relations are learned by a classifier instead. Because the main intervention at classifier training time is simply a reordering of samples, it makes our method lightweight and highly flexible, enabling seamless incorporation with off-the-shelf domain generalization methods [17–19]. The simplicity of the intervention enables useful theoretical guarantees, and the sophisticated learned variational autoencoders (VAE) that drive the intervention ensure an ability to demonstrable utility via performance gains over previously established baselines.

Our contributions are as follows: (1) We propose a general causality-based framework for the domain generalization problem of classification tasks; (2) We prove that a spurious-free *balanced distribution* can produce mimmax optimal classifiers for OOD generalization; (3) We demonstrate that the source of spurious correlation, as a latent variable, can be identified given a large enough set of training environments under mild conditions in a nonlinear setting; (4) We propose a novel balanced mini-batch sampling algorithm that, in an ideal scenario with exact matches of the true source of spurious correlation, can remove the spurious correlations in the observed data distribution; (5) Our empirical results show that our two-phased method obtains significant performance gain on three domain generalization datasets, ColoredMNIST [12], PACS [20] and TerraIncognita [21], across four different domain generalization methods over a random sampling strategy.

2 Preliminaries

2.1 Problem Setting

We consider a standard domain generalization setting with a potentially high-dimensional variable X (e.g. an image), a label variable Y and a discrete environment (or domain) variable E in the sample spaces $\mathcal{X}, \mathcal{Y}, \mathcal{E}$, respectively. Here we focus on the classification problems with $\mathcal{Y} = \{1, 2, \dots, m\}$ and $\mathcal{X} \in \mathbb{R}^d$. We assume that the training data are collected from a finite subset of training environments $\mathcal{E}_{\text{train}} \subset \mathcal{E}$. The training data $\mathcal{D}^e = \{(x_i^e, y_i^e)\}_{i=1}^{N^e}$ is then sampled from the distribution $p^e(X, Y) = p(X, Y|E = e)$ for all $e \in \mathcal{E}_{\text{train}}$. Our goal is to learn a classifier $C_\psi : \mathcal{X} \rightarrow \mathcal{Y}$ that performs well in a new, unseen environment $e_{\text{test}} \notin \mathcal{E}_{\text{train}}$.

We assume that there is a data generation process of the observed data distribution $p^e(X, Y)$ represented by an underlying structural causal model (SCM) shown in fig. 1a. More specifically, we assume that X is caused by label Y , an unobserved latent variable Z (with sample space $\mathcal{Z} \in \mathbb{R}^n$) and an independent noise variable ϵ with the following formulation:

$$X = \mathbf{f}(Y, Z) + \epsilon = \mathbf{f}_Y(Z) + \epsilon \quad (1)$$

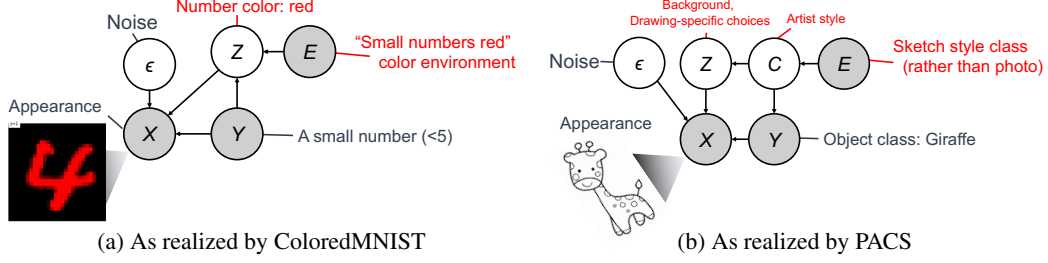


Figure 2: Annotated example causal graphs of two realizations of the joint distribution $p(X, Y, E)$.

Here, we assume the causal mechanism is invariant across all environments $e \in \mathcal{E}$ and we further characterize \mathbf{f} with the following assumption:

Assumption 1. $\mathbf{f} : \{1, 2, \dots, m\} \times \mathcal{Z} \rightarrow \mathcal{X}$ is injective. $\mathbf{f}^{-1} : \mathcal{X} \rightarrow \{1, 2, \dots, m\} \times \mathcal{Z}$ is the left inverse of \mathbf{f} .

Note that this assumption forces the generation process of X to consider both Z and Y instead of only one of them. Suppose ϵ has a known probability density function $p_\epsilon > 0$. Then we have

$$p_{\mathbf{f}}(X|Z, Y) = p_\epsilon(X - \mathbf{f}_Y(Z)) \quad (2)$$

While the causal mechanism is invariant across environments, we assume that the correlation between label Y and latent Z is environment-variant and Z should exclude Y information. i.e., Y cannot be recovered as a function of Z . If Y is a function of Z , the generation process of X can completely ignore Y and \mathbf{f} would not be injective. Let $e \in \mathcal{E}$ index a family of distributions $\mathcal{F} = \{p^e(X, Y, Z) = p_{\mathbf{f}}(X|Z, Y)p^e(Z|Y)p^e(Y)\}_e$, where $p^e(Z|Y) > 0$ and $p^e(Y) > 0$. Note that any mixture of distributions from \mathcal{F} would also be a member of \mathcal{F} .

In this setting, we can see that the correlation between X and Y would vary for different values of e . We argue that the correlation $Y \leftrightarrow Z \rightarrow X$ is not stable in an unseen environment $e \notin \mathcal{E}_{\text{train}}$ as it involves E and we only want to learn the stable causal relation $Y \rightarrow X$. However, it is inevitable that the learned predictor may absorb the unstable relation between X and Y if we simply train it on the observed train distribution $p^e(X, Y)$ with empirical risk minimization.

For example, consider the image classification domain. Under this causal model of data production an image X of an object in class Y has an appearance driven by the fundamental shared properties of Y as well as a potentially massive set of meaningful latent features Z that do not determine “ Y -ness” that can be spuriously correlated with environment E . To assess techniques to mitigate spurious correlations in vision tasks, challenge datasets with shifting spurious correlations between the training and test environments such as ColoredMNIST [12] and PACS [20] have been proposed. We plot causal diagrams for these two datasets’ joint distributions $p(X, Y, E)$ in Figure 2. Scenario (a) shows the data generation process of ColoredMNIST, with Z indicating the assigned color, which is determined by the digit label Y and the environment $E = p(Z|Y)$. Scenario (b) can be regarded as the data generation process of datasets like PACS, where images of the same objects in multiple styles (e.g. sketches and photographs) occur, with Z containing this stylistic information. In short, our goal is to robustly learn a classifier that can correctly identify, for (a) the class a number form belongs to without leveraging unreliable color information and (b) what object is being depicted in an image without relying on the style it is depicted in. While the specific example tasks we consider in this work are all in the image classification domain, the theoretical setting, techniques we propose, and guarantees we make generalize to other classification problems.

2.2 Balanced Distribution

To avoid learning the unstable relations, we propose to consider a balanced distribution $p^B(X, Y, Z)$ such that $Y \perp\!\!\!\perp_B Z$ while the causal mechanism $Z \rightarrow X \leftarrow Y$ unchanged, as shown in fig. 1b, which is defined below:

Definition 1. A *balanced distribution* can be written as $p^B(X, Y, Z) = p_{\mathbf{f}}(X|Y, Z)p^B(Z)p^B(Y)$, where $p^B(Y) = U\{1, 2, \dots, m\}$ and $Y \perp\!\!\!\perp_B Z$.

In this new distribution, X and Y is only correlated through the stable causal relation $Y \rightarrow X$. Here we do not specify $p^B(Z)$. Note that $p^B(X|Y, Z) = p_f(X|Y, Z)$ is a result of the unchanged causal mechanism $Z \rightarrow X \leftarrow Y$, and that $p^B(X, Y, X) \in \mathcal{F}$ can also be regarded as from an environment $B \in \mathcal{E}$. Under an additional conditional independence assumption $Y \perp\!\!\!\perp_B Z|X$, we can prove that $p^B(Y|X)$ is invariant for any choice of $p^B(Z)$. Then we have the following theorem¹:

Theorem 1. Consider a classifier $C_\psi(X) = \arg \max_Y p_\psi(Y|X)$ with parameter ψ . We denote the cross entropy loss of such a classifier on environment e by $L^e(p_\psi(Y|X)) = -\mathbb{E}_{p^e(X, Y)} \log p_\psi(Y|X)$. Assume that (1) $Y \perp\!\!\!\perp_B Z|X$, and (2) \mathcal{E} satisfies:

$$\forall e \in \mathcal{E}, Y \not\perp\!\!\!\perp_{p^e} Z \implies \exists e' \in \mathcal{E} \text{ s.t. } L^{e'}(p^e(Y|X)) - L^{e'}(p^B(Y)) > 0 \quad (3)$$

Then the Bayes optimal classifier trained on any balanced distribution $p^B(X, Y)$ is a **minimax optimal classifier** with respect to cross entropy loss across all environments in \mathcal{E} :

$$p^B(Y|X) = \operatorname{argmin}_{p_\psi \in \mathcal{F}} \max_{e \in \mathcal{E}} L^e(p_\psi(Y|X)) \quad (4)$$

The first assumption implies the noise variable ϵ can be disentangled into (ϵ_Y, ϵ_Z) , such that there exist functions $\mathbf{g}_Y, \mathbf{g}_Z$ with $(Y, Z) = \mathbf{f}^{-1}(X - \epsilon) = (\mathbf{g}_Y(X - \epsilon_Y), \mathbf{g}_Z(X - \epsilon_Z))$. The second assumption implies that the environment space \mathcal{E} is large and diverse enough such that a perfect classifier on one environment will always perform worse than random guessing on some other environment. Under these two assumptions, no other Byes optimal classifier produced by an environment in \mathcal{E} would have a better worst case OOD performance than the balanced distribution.

3 Method

We propose a two-phased method that first use an VAE to learn the underlying data distribution $p^e(X, Y, Z)$ with latent covariate Z for each $e \in \mathcal{E}_{\text{train}}$, and then use the learned distribution to calculate a balancing score to create a balanced distribution based on the training data.

3.1 Latent Covariate Learning

We argue that the underlying joint distribution of $p^e(X, Y, Z)$ can be learned and identified by a VAE, given a sufficiently large set of train environments $\mathcal{E}_{\text{train}}$.

To specify the correlation between Z and Y , we assume that the conditional distribution $p^e(Z|Y)$ is conditional factorial with an exponential family distribution:

Assumption 2. The correlation between Y and Z in environment e is characterized by $p_{T, \lambda}^e(Z|Y)$ as follows:

$$p_{T, \lambda}^e(Z|Y) = \prod_{i=1}^n \frac{Q_i(Z_i)}{W_i^e(Y)} \exp \left[\sum_{j=1}^k T_{ij}(Z_i) \lambda_{ij}^e(Y) \right] \quad (5)$$

where Z_i is the i -th element of Z , $\mathbf{Q} = [Q_i]_i : \mathcal{Z} \rightarrow \mathbb{R}^n$ is the base measure, $\mathbf{W}^e = [W_i^e]_i : \mathcal{Y} \rightarrow \mathbb{R}^n$ is the normalizing constant, $\mathbf{T} = [T_{ij}]_{ij} : \mathcal{Z} \rightarrow \mathbb{R}^{nk}$ is the sufficient statistics, and $\lambda^e = [\lambda_{ij}^e]_{ij} : \mathcal{Y} \rightarrow \mathbb{R}^{nk}$ are the Y dependent parameters.

Here n is the dimension of the latent variable Z , and k is the dimension of each sufficient statistic determined by the type of chosen exponential family distribution. The simplified conditional factorial prior assumption is from the mean-field approximation, which can be expressed as a closed form of the true prior [22]. Note that the exponential family assumption is not very restrictive as it has universal approximation capabilities [23].

We then consider the following conditional generative model in each environment $e \in \mathcal{E}_{\text{train}}$, with parameters $\theta = (\mathbf{f}, \mathbf{T}, \lambda)$:

$$p_\theta^e(X, Z|Y) = p_f(X|Z, Y) p_{T, \lambda}^e(Z|Y) \quad (6)$$

We use a VAE to estimate the above generative model with a variational approximation $q_\phi^e(Z|X, Y)$ of the prior probability of latent variable $p_\theta^e(Z|X, Y)$. We denote the empirical data distribution given

¹See appendix A for all the proofs.

by dataset $\mathcal{D}^e = \{(x_i^e, y_i^e)\}_{i=1}^{N^e}$ collected from environment e . The evidence lower bound (ELBO) of the data log-likelihood in each environment $e \in \mathcal{E}_{\text{train}}$ is then defined as follows:

$$\mathbb{E}_{q_{\mathcal{D}^e}} [\log p_{\theta}^e(X|Y)] \geq \mathcal{L}^e(\theta, \phi) := \mathbb{E}_{q_{\mathcal{D}^e}} [\mathbb{E}_{q_{\phi}^e(Z|X, Y)} [\log p_{\theta}(X|Z, Y)] - KL(q_{\phi}^e(Z|X, Y) || p_{\theta}^e(Z|Y))] \quad (7)$$

The KL-divergence term can be calculated analytically. To sample from the variational distribution $q_{\phi}^e(Z|X, Y)$, we use reparameterization trick [24].

We then maximize the above ELBO $\frac{1}{|\mathcal{E}_{\text{train}}|} \sum_{e \in \mathcal{E}_{\text{train}}} \mathcal{L}^e(\theta, \phi)$ over all training environments to obtain model parameters (θ, ϕ) . To show that we can uniquely recover the latent variable Z up to some simple transformations, we want to show that the model parameter θ is identifiable up to some simple transformations. That is, for any $\{\theta = (\mathbf{f}, \mathbf{T}, \lambda), \theta' = (\mathbf{f}', \mathbf{T}', \lambda')\} \in \Theta$,

$$p_{\theta}^e(X|Y) = p_{\theta'}^e(X|Y), \forall e \in \mathcal{E}_{\text{train}} \implies \theta \sim \theta' \quad (8)$$

where Θ is the parameter space and \sim represents an equivalent relation. Specifically, we consider the following equivalence relation from [25]:

Definition 2. If $(\mathbf{f}, \mathbf{T}, \lambda) \sim_A (\mathbf{f}', \mathbf{T}', \lambda')$, then there exists an invertible matrix $A \in \mathbb{R}^{nk \times nk}$ and a vector $\mathbf{c} \in \mathbb{R}^{nk}$, such that $\mathbf{T}(\mathbf{f}^{-1}(x)) = A\mathbf{T}'(\mathbf{f}'^{-1}(x)) + \mathbf{c}, \forall x \in \mathcal{X}$.

When the underlying model parameter θ^* can be recovered by perfectly fitting the data distribution $p_{\theta^*}^e(X|Y)$ for all $e \in \mathcal{E}_{\text{train}}$, the joint distribution $p_{\theta^*}^e(X, Z|Y)$ is also recovered. This further implies the recovery of the prior $p_{\theta^*}^e(Z|Y)$ and the true latent variable Z^* .

The identifiability of our proposed latent covariate learning model can then be summarized as follows:

Theorem 2. Suppose we observe data sampled from the generative model defined according to eq. (6), with parameters $\theta = (\mathbf{f}, \mathbf{T}, \lambda)$. In addition to assumption 1 and assumption 2, we assume the following conditions holds: (1) The set $\{x \in \mathcal{X} | \phi_{\epsilon}(x) = 0\}$ has measure zero, where ϕ_{ϵ} is the characteristic function of the density p_{ϵ} . (2) The sufficient statistics T_{ij} are differentiable almost everywhere, and $(T_{ij})_{1 \leq j \leq k}$ are linearly independent on any subset of \mathcal{X} of measure greater than zero. (3) There exist $nk + 1$ distinct points $(y_0, e_0), \dots, (y_{nk}, e_{nk})$ such that the $nk \times nk$ matrix

$$\mathbf{L} = (\lambda^{e_1}(y_1) - \lambda^{e_0}(y_0), \dots, \lambda^{e_{nk}}(y_{nk}) - \lambda^{e_0}(y_0)) \quad (9)$$

is invertible. Then we have the parameters $\theta = (\mathbf{f}, \mathbf{T}, \lambda)$ are \sim_A -identifiable.

Note that the last assumption in theorem 2 implies that the product space $\mathcal{Y} \times \mathcal{E}_{\text{train}}$ has to be large enough to ensure the identifiability of θ when perfectly fitting the given training data distribution. i.e. We need $m|\mathcal{E}_{\text{train}}| > nk$. The invertibility of \mathbf{L} implies that $\lambda^{e_i}(y_i) - \lambda^{e_0}(y_0)$ need to be orthogonal to each other which further implies the diversity of environment space \mathcal{E} .

3.2 Balanced mini-batch sampling

We consider a classic method that has been widely used in the average treatment effect (ATE) estimation — balancing score matching — to sample balanced mini-batches that mimic a balanced distribution shown in fig. 1b.

Causal effect estimation studies the effect a treatment would have had on a unit which in reality received another treatment. A causal graph similar to fig. 1a is usually considered in a causal effect estimation problem, where Z is called the covariate (e.g. a patient profile), which is observed before treatment $Y \in \{0, 1\}$ (e.g. taking drug or placebo) is applied. We denote the effect of receiving a specific treatment $Y = y$ as X_y . Note that this causal graph implies that we make the Strong Ignorability assumption. i.e. Z includes all variables that are related to both X and Y .

In the case of a binary treatment, the ATE is defined as the expected difference of effect after receiving different treatments: $\mathbb{E}[X_1 - X_0]$ (e.g. difference in blood pressure). For a randomized controlled trial, we can directly estimate the difference between $\mathbb{E}[X|Y = 1]$ and $\mathbb{E}[X|Y = 0]$ from the observed data as the true treatment effect, as in this case we force $Z \perp\!\!\!\perp Y$ and there would not be systematical difference between units exposed to one treatments and units exposed to another.

However, in most observed datasets, Z is correlated with Y . Thus $\mathbb{E}[X|Y = 1]$ and $\mathbb{E}[X|Y = 0]$ are not directly comparable. We can then use balancing score $b(Z)$ [26] to de-correlate Z and Y :

Definition 3. A **balancing score** $b(Z)$ is a function of covariate Z s.t. $Z \perp\!\!\!\perp Y | b(Z)$.

Algorithm 1: Balanced Mini-batch sampling.

Input: $|\mathcal{E}_{\text{train}}|$ training datasets $\mathcal{D}^e = \{(x_i^e, y_i^e)\}_{i=1}^{N^e}$ sampled from distribution $P(X, Y|E = e)$ for all $e \in \mathcal{E}_{\text{train}}$, a balancing score $b^e(z_i)$ calculated for each training data point (x_i^e, y_i^e) , and a distance metrics $d(\cdot, \cdot)$ that calculates the distance between two balancing scores;
Output: A balanced batch of data D_{balanced} consisting of $B \times |\mathcal{E}_{\text{train}}| \times (a + 1)$ examples;
 $D_{\text{balanced}} \leftarrow \text{Empty};$
for $e \in \mathcal{E}_{\text{train}}$ **do**
 Randomly sample B data points D_{random}^e from \mathcal{D}^e ;
 Add D_{random}^e to D_{balanced} ;
 for $(x^e, y^e) \in D_{\text{random}}^e$ **do**
 Uniformly sample a different labels Y_{alt} from $\mathcal{Y} = \{1, 2, \dots, m\}$ such that $y \neq y^e$ for all $y \in Y_{\text{alt}}$;
 Suppose the balancing score of (x^e, y^e) is $b^e(z)$;
 for $y \in Y_{\text{alt}}$ **do**
 Search across \mathcal{D}^e for the data point (x_j^e, y_j^e) such that $y_j^e = y$ and has the smallest $d(b^e(z_j), b^e(z))$;
 Add (x_j^e, y_j^e) to D_{balanced} ;

The ATE can then be estimated by matching units with same balancing score but different treatments: $\mathbb{E}_{b(Z)} [\mathbb{E}[X|Y = 1, b(Z)] - \mathbb{E}[X|Y = 0, b(Z)]]$. There is a wide range of functions of Z that can be used as a balancing score, where the scalar propensity score $p(Y = 1|Z)$ is the coarsest one and the covariate Z itself is the finest one [27]. To extend this statement to non-binary treatments, we first define propensity score $s(Z)$ for $Y \in \mathcal{Y} = \{1, 2, \dots, m\}$ as a vector:

Definition 4. The *propensity score* for $Y \in \{1, 2, \dots, m\}$ is $s(Z) = [p(Y = y|Z)]_{y=1}^m$.

We then have the following theorem that applies to the vector version of propensity score $s(Z)$:

Theorem 3. Let $b(Z)$ be a function of Z . Then $b(Z)$ is a balancing score, if and only if $b(Z)$ is finer than $s(Z)$. i.e. exists a function g such that $s(Z) = g(b(Z))$.

We use $b^e(Z)$ to denote the balancing score for a specific environment e . The propensity score in a training environment e would then be $s^e(Z) = [p_{\theta}^e(Y = y|Z)]_{y=1}^m$, which can be derived from the learned conditional prior $p_{\theta}^e(Z|Y)$:

$$p_{\theta}^e(Y = y|Z) = \frac{p_{\theta}^e(Z|Y = y)p^e(Y = y)}{\sum_{i=1}^m p_{\theta}^e(Z|Y = i)p^e(Y = i)} \quad (10)$$

where $p^e(Y = i)$ can be directly estimated from the training data \mathcal{D}^e .

We propose to construct balanced mini-batches by matching $1 \leq a \leq m - 1$ examples with a different label Y but the same/closest balancing score $b^e(Z)$ for each example sampled from the training environment e . The detailed sampling algorithm is shown in Algorithm 1.

With perfect match at every step (i.e., $b^e(z_j) = b^e(z)$) and $a = m - 1$, we can obtain a completely balanced mini-batch sampled from the balanced distribution with $Y \perp\!\!\!\perp Z$. However, an exact match of balancing score is unlikely in reality, so the quality of matched data point would likely be lower than the referencing data point in terms of having the same balancing score. This can be mitigated by choosing a smaller a . However, this would make Y and Z not completely independent. In fact, if we have exact match of balancing score, the larger a is, the weaker the correlation between Y and Z would be. So in practice, the choice of a reflects a trade-off between the balancing score matching quality and the degree of dependency between Y and Z . The above arguments can be summarized as below:

Theorem 4. A balanced mini-batch with exact matches of balancing score and $a = m - 1$ can be regarded as sampling from the balanced distribution over all training environments $p^B(X, Y, Z)$. In general, the balanced mini-batch can be regarded as sampling from a semi-balanced distribution with $\hat{p}^B(Y|Z, E) = \frac{1}{a+1}(\frac{a}{m-1} + \frac{m-a-1}{m-1}p(Y|Z, E))$.

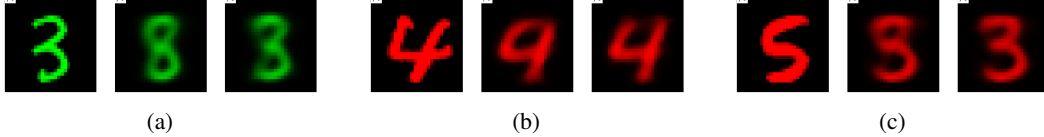


Figure 3: Reconstructed ColoredMNIST images from our VAE model. In each sub-figure, we infer Z from the leftmost image, then generate images with label $Y = 0$ (middle) and $Y = 1$ (right).

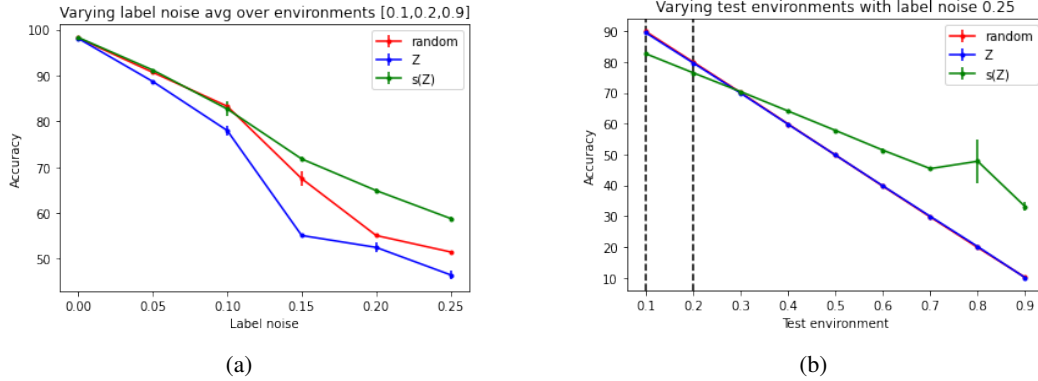


Figure 4: We plot the test accuracy on ColoredMNIST dataset versus varying (a) label noise and (b) test environments. The vertical bars indicate variance over 3 runs. In figure (a) we report the averaged test accuracy as in the last column of table 1. In figure (b), we use $p(\text{Color}=\text{Red}|Y = 1) = 0.1, 0.2$ as train environments and we can see that the propensity score matching method ($s(Z)$) consistently outperform the random baseline when the test environment gets harder.

4 Experiments

To verify the effectiveness of our proposed balancing mini-batch method, we conduct experiments on three datasets exhibiting spurious correlations: **ColoredMNIST** [12], **PACS** [20] and **TerraIncognita** [21]. Each dataset has multiple environments, which we use as unseen test environments to report the test accuracy while the other environments serve as the training environments.

Our method only modifies the mini-batch sampling strategy and complement any established domain generalization method. Thus we applied our proposed balanced mini-batch sampling method along with four widely-used domain generalization baselines: **ERM** [28], **IRM** [17], **GroupDRO** [18] and **CORAL** [19], and compare the performance of using our balanced mini-batch sampling strategy with using the usual random mini-batch sampling strategy.

Empirical risk minimization (ERM) is a default training scheme for most machine learning problems, merging all training data into one dataset and minimizing the training errors across all training domains. Invariant risk minimization (IRM) learns a data representation such that the optimal linear classifier on top of it is invariant across training domains. Group distributionally robust optimization (GroupDRO) performs ERM while increasing the weight of the environments with larger errors. Deep CORAL matches the mean and covariance of feature distributions across training domains.

We perform our experiments on the DomainBed codebase² and follow its default settings. We use the training-domain validation as defined in [17] for model selection, i.e., we choose the model that maximizes the accuracy on the union of validation sets from all the training domains. We use a multi-layer perceptron based VAE [24] to learn the latent covariate Z and we choose the conditional prior $p_{\theta}(Z|Y, E = e)$ to be a Gaussian distribution with diagonal covariance matrix. We also choose the noise distribution p_{ϵ} to be a Gaussian distribution with zero mean and fixed variance. For the architecture of the image classifiers (ERM [28], IRM [17], GroupDRO [18], CORAL [19]), following the setting of DomainBed [17], we train a convolutional neural network from scratch for ColoredMNIST [12] dataset, and use a pretrained ResNet50 [29] for PACS [20] and TerraIncognita [21]. For choosing the hyperparameters of the classifiers, we show the results with two sets of hyperparameters: the optimal hyperparameters selected for the reported results in the

²<https://github.com/facebookresearch/DomainBed>

Table 1: Out-of-domain test accuracy on ColoredMNIST dataset. Numbers are averaged over 3 runs with standard deviation.

	Sampling	Algorithm	0.1	0.2	0.9	Avg
Reported hyperparameters	Random	ERM	72.2 \pm 0.4	73.5 \pm 0.2	10.0 \pm 0.1	51.9 \pm 0.5
		IRM	73.0 \pm 0.0	73.4 \pm 0.1	9.8 \pm 0.2	52.1 \pm 0.1
		GroupDRO	72.8 \pm 0.5	73.4 \pm 0.1	10.0 \pm 0.2	52.1 \pm 0.3
		CORAL	71.3 \pm 0.3	73.1 \pm 0.4	10.5 \pm 0.0	51.6 \pm 0.1
	Balanced $b(Z) = Z$	ERM	63.9 \pm 1.6	67.4 \pm 1.4	10.4 \pm 0.4	47.2 \pm 1.1
		IRM	65.5 \pm 1.7	64.9 \pm 0.2	10.0 \pm 0.1	46.8 \pm 0.7
		GroupDRO	63.9 \pm 0.1	65.3 \pm 0.4	9.8 \pm 0.1	46.4 \pm 0.1
		CORAL	66.0 \pm 1.1	66.1 \pm 1.4	10.1 \pm 0.1	47.4 \pm 0.9
	Balanced $b(Z) = s^e(Z)$	ERM	71.6 \pm 0.5	70.8 \pm 0.2	31.5 \pm 3.3	58.0 \pm 1.3
		IRM	70.4 \pm 0.6	72.5 \pm 0.3	10.9 \pm 0.6	51.3 \pm 0.4
		GroupDRO	70.4 \pm 0.6	72.4 \pm 0.1	27.5 \pm 3.2	56.7 \pm 0.9
		CORAL	72.0 \pm 0.5	72.2 \pm 0.6	33.4 \pm 2.9	59.2 \pm 1.0
Default hyperparameters	Random	ERM	71.8 \pm 0.2	72.5 \pm 0.1	10.1 \pm 0.1	51.5 \pm 0.1
		IRM	59.8 \pm 1.5	58.1 \pm 1.8	9.7 \pm 0.0	42.5 \pm 1.0
		GroupDRO	72.7 \pm 0.2	73.0 \pm 0.2	10.0 \pm 0.2	51.9 \pm 0.0
		CORAL	71.4 \pm 0.2	72.8 \pm 0.1	9.9 \pm 0.0	51.4 \pm 0.1
	Balanced $b(Z) = Z$	ERM	63.5 \pm 2.2	66.0 \pm 0.8	10.0 \pm 0.1	46.5 \pm 0.9
		IRM	54.4 \pm 8.4	69.4 \pm 7.5	9.9 \pm 0.2	44.6 \pm 4.7
		GroupDRO	65.7 \pm 1.5	67.1 \pm 1.8	14.9 \pm 4.0	49.2 \pm 0.7
		CORAL	64.7 \pm 0.8	65.5 \pm 0.9	14.9 \pm 4.1	48.4 \pm 1.7
	Balanced $b(Z) = s^e(Z)$	ERM	72.1 \pm 0.1	71.2 \pm 0.2	33.1 \pm 1.3	58.8 \pm 0.5
		IRM	69.8 \pm 0.6	62.2 \pm 5.6	10.9 \pm 0.5	47.6 \pm 1.6
		GroupDRO	72.3 \pm 0.2	71.4 \pm 0.6	25.9 \pm 6.7	56.6 \pm 2.2
		CORAL	72.0 \pm 0.6	71.8 \pm 0.6	32.1 \pm 0.7	58.6 \pm 0.2

DomainBed [17] paper and the default hyperparameters settings in their code base. Each experiment is repeated with 3 different random seeds.

In the experiments below, we use both $b(Z) = Z$ and $b(Z) = s^e(Z)$ to construct balanced mini-batches, and we call these two variants of our method *covariate matching* and *propensity score matching*, respectively. For all datasets, we set the number of matched examples to be $a = 1$.

ColoredMNIST. The ColoredMNIST [12] dataset is generated from the regular MNIST hand-written digits dataset [30] by first assigning a binary label to indicate whether the digit is smaller than 5 to each MNIST image with some random noise, and then assigning a binary color (green or red) based on different correlations with the label across environments. Because of the injected noise in label assignment, the maximum accuracy a classifier can achieve is 75%. As shown in Table 1, there are in total 3 environments in the dataset, each of which has $p(\text{Color}=\text{Red}|Y = 1) = 0.1, 0.2, 0.9$, with 70,000 examples in each environment. In this case we have $|\mathcal{E}_{\text{train}}| = 2$ and $m = 2$. We also set $k = 1$ by fixing the variance of the conditional prior $p_{\theta}(Z|Y, E = e)$ to be 1. Then we take the maximum possible dimension of the latent Z , $n = 3$, according to the identifiability condition in Theorem 2. Note that as $m = 2$, the balanced mini-batches can be regarded as sampling from a balanced distribution with perfect match in balancing score and $a = 1$ as stated in Theorem 4.

Figure 3 shows three sets of reconstructed images with the same latent variable Z and different label Y using our VAE model. We can see that Z keeps the color feature and some style features, while the digit shape is changed with corresponding label Y .

As shown in Table 1, our proposed balanced mini-batch sampling method significantly outperforms random mini-batch sampling in the worst test environment (0.9) by 20% (absolute), while achieving comparable performance on the other two environments. the propensity score matching method ($s(Z)$) obtain more performance gain on harder environments as shown in fig. 4b. Note that the best averaged score on ColoredMNIST reported by [17] over 14 domain generalization baselines is 56.2% (ARM [31]), which is still lower than our balanced ERM result (58.8%). On ColoredMNIST, the propensity score matching method ($b(Z) = s^e(Z)$) significantly outperforms the covariate matching matching method ($b(Z) = Z$), and out performs the random mini-batch sampling baseline by more

Table 2: Out-of-domain test accuracy on PACS and TerraIncognita dataset. Numbers are averaged over all test environments with 3 runs with standard deviation.

Sampling	Algorithm	Reported hyperparameters		Default hyperparameters	
		PACS	TerraIncognita	PACS	TerraIncognita
Random	ERM	85.3 \pm 1.3	42.9 \pm 2.6	83.7 \pm 0.1	46.1 \pm 1.2
	IRM	82.2 \pm 1.0	38.3 \pm 1.1	81.2 \pm 0.4	39.3 \pm 1.8
	GroupDRO	82.5 \pm 1.2	42.8 \pm 3.2	83.7 \pm 0.4	43.6 \pm 1.2
	CORAL	79.1 \pm 5.2	40.5 \pm 5.8	84.8 \pm 0.2	44.8 \pm 0.3
Balanced $b(Z) = Z$	ERM	83.0 \pm 0.1	45.2 \pm 2.6	85.2 \pm 0.3	47.1 \pm 0.6
	IRM	80.5 \pm 0.6	40.7 \pm 2.8	82.6 \pm 0.3	40.1 \pm 1.4
	GroupDRO	85.1 \pm 2.8	42.2 \pm 2.6	84.7 \pm 0.6	41.6 \pm 1.5
	CORAL	86.1 \pm 3.4	42.9 \pm 1.9	84.3 \pm 0.5	47.3 \pm 0.4
Balanced $b(Z) = s^e(Z)$	ERM	84.1 \pm 0.6	46.3 \pm 1.5	85.2 \pm 0.4	48.1 \pm 0.3
	IRM	82.1 \pm 0.7	39.3 \pm 3.8	82.1 \pm 0.6	40.2 \pm 2.9
	GroupDRO	82.2 \pm 0.7	42.3 \pm 1.9	84.3 \pm 0.4	43.1 \pm 0.6
	CORAL	85.3 \pm 2.5	43.2 \pm 2.3	85.1 \pm 0.4	46.2 \pm 0.4

than 5% (absolute) with all four classifiers. This is likely due to the relatively large noise (25%) in the label assignment: Z captures all other features except the ones directly determines the label, while $s^e(Z)$ only capture the features that has strong correlation with the label Y . i.e. the color information. As Z is finer and contains more information than $s^e(Z)$, it is likely that the closest match by $b(Z) = Z$ would be an image of the same digit with the same color. i.e. The matched example is likely to be an image labeled with the “wrong” class. This will hurt the performance as we are up-sampling the noise data.

PACS and TerraIncognita. We also conduct experiments on two more realistic datasets, PACS [20] and TerraIncognita [21]. The PACS dataset has four environments, each indicates an image style: art, cartoons, photos and sketches, with 9,991 examples in total. There are 7 classes in the dataset, indicating the object in the image. The TerraIncognita dataset contains photographs of wild animals taken by camera traps at four different locations: L100, L38, L43 and L46, with 24,788 examples in total. There are 10 classes in the dataset, indicating the animal appears in the image.

In these two datasets, we do not require $|\mathcal{E}_{\text{train}}|$, m , n and k to explicitly satisfy the identifiability condition in Theorem 2, as the latent variable could require a larger dimensionality n to capture than the dataset allows. Also, as $m > 2$, $a = 1$ means we cannot completely eliminate the spurious correlation in the training dataset in the ideal scenario. Even given these non-ideal conditions, in Table 2, our experiments show that our balanced mini-batch sampling can significantly outperform the random mini-batch sampling baseline with different domain generalization baselines. On these two real-world datasets, we observe that the performance difference between covariate matching and propensity score matching is not as large as that on the ColoredMNIST dataset. It is partially because these two datasets have less label noise than ColoredMNIST. We only report the average accuracy over all test environments. Detailed results on each test environment can be found in Appendix C.

5 Discussions and Limitations

The experiments show that our balanced mini-batch sampling method outperforms the random mini-sampling baseline when applied to multiple domain generalization methods, on both semi-synthetic datasets and real-world datasets. While our method can be easily incorporated to other domain generalization methods with good performance, there are some potential drawbacks of our method. First, our method is sensitive to dataset size. A reasonable amount of data in each class is needed to learn the latent Z and find good matches with respect to a specific value of balancing score. On the other hand, if the dataset size is too big, searching across the whole dataset to find the closest match in balancing score becomes time-inefficient. However, this could be solved by matching examples offline before training, or with more efficient searching methods. The second caveat is that we do not provide an optimized model selection method to complement our method. While we could also balance the held-out validation set with our method and choose the best model based on the accuracy on the balanced validation set, the quality of such a balanced validation set is questionable given the small size of a typical validation set. We used the common training-domain validation scheme.

6 Related Work

A growing body of work has investigated the out-of-domain (OOD) generalization problem with causal modeling. One prominent idea is to learn invariant causal features that describe the true causal mechanism of interest across domains.

When multiple training domains are available, this can be approximated by enforcing some invariance conditions across training domains by adding a regularization term to the usual empirical risk minimization [12, 32, 33, 16]. Invariant risk minimization (IRM) [12] seeks to find a data representation such that the predictor using the representation is invariant across all environments. Risk extrapolation (REx) [32] encourages the training risks in different domains to be similar, while derivative invariant risk minimization (DIRM) [33] encourages the invariance of the gradient of training risks across different domains. Another possible invariant condition is multi-domain calibration [16], which aims to learn a calibrated predictor on all domains. However, recent work claims that many of these approaches still fail to achieve the intended invariance property [34–36], and thorough empirical study questions the true effectiveness of these domain generalization methods [17].

Instead of using datasets from multiple domains, some works propose to use an auxiliary variable different from the label to solve the OOD problem [37, 38]. In this case, only one train domain is required. Their methods are two-phased that (1) balance the train data distribution with the help of auxiliary variable; and (2) add invariance regularizations on the training objective. Our method is comparable to their first phase, but utilizes multiple training domains instead of an auxiliary variable. We are using a matching based method to produce the balanced distribution instead of reweighting the train data [37, 38] or model the train distribution with a generative model (without identifiability guarantee) [38].

Instead of using an observed auxiliary variable or multiple training domains, some other OOD works propose to use VAE to learn latent variables in the assumed causal graph [14, 15], with appropriate assumptions of the train data distribution. Causal Semantic Generative model (CSG) [14] aims to disentangle the semantic features that cause both the label Y and the image X and non-semantic features that only cause X . Invariant Causal Representation Learning (iCaRL) [15] makes a similar but more fine grained assumption on the latent variables and tries to find the ones cause Y by causal discovery. The identifiability of such latent variables is usually based on the pioneer work on identifiable VAE by [39], which assumes that the latent variable has a factorial exponential family distribution given an auxiliary variable. Our identifiability result is also an extension of [39], where we use labels and training domains as the auxiliary variable and include the label Y in the causal mechanism of generating X instead of only using the latent variable Z to generate X .

Our method is based on the idea of both distribution balancing and latent variable learning. To better utilize the learned latent variable, we use a classic method for average treatment effect (ATE) estimation [40] – balancing score matching [27]. Recently, perfect match [41] extends this method to individual treatment effect (ITE) estimation [40] by constructing virtually randomized mini-batches with balancing score, which is similar to our method. However, as described in section 3.2, treatment effect estimation is an essentially different task from classification, as in treatment effect estimation, Z is observed and we are interested in the difference of X when different Y is applied.

7 Conclusion

Our novel causality-based domain generalization method for classification tasks samples balanced mini-batches to reduce the presentation of spurious correlations in the dataset. We propose a spurious-free balanced distribution and show that the Bayes optimal classifier trained on such distribution is minimax optimal over all environments. We show that our assumed data generation model with invariant causal mechanism can be identified up to sample transformations. We demonstrate theoretically that the balanced mini-batch is approximately sampled from a spurious-free balanced distribution with the same causal mechanism under ideal scenarios. Our experiments empirically show the effectiveness of our method in both a semi-synthetic setting that strictly follows our assumptions and the real-world setting that loosely satisfies our assumptions.

References

- [1] Silver, D., A. Huang, C. J. Maddison, et al. Mastering the game of go with deep neural networks and tree search. *nature*, 529(7587):484–489, 2016.
- [2] Devlin, J., M.-W. Chang, K. Lee, et al. Bert: Pre-training of deep bidirectional transformers for language understanding. In *Proceedings of the 2019 Conference of the North American Chapter of the Association for Computational Linguistics: Human Language Technologies, Volume 1 (Long and Short Papers)*, pages 4171–4186. 2019.
- [3] Jumper, J., R. Evans, A. Pritzel, et al. Highly accurate protein structure prediction with alphafold. *Nature*, 596(7873):583–589, 2021.
- [4] Quiñero-Candela, J., M. Sugiyama, N. D. Lawrence, et al. *Dataset shift in machine learning*. Mit Press, 2009.
- [5] Szegedy, C., W. Zaremba, I. Sutskever, et al. Intriguing properties of neural networks, 2014.
- [6] Jo, J., Y. Bengio. Measuring the tendency of cnns to learn surface statistical regularities, 2017.
- [7] Geirhos, R., P. Rubisch, C. Michaelis, et al. Imagenet-trained cnns are biased towards texture; increasing shape bias improves accuracy and robustness, 2019.
- [8] Beery, S., G. Van Horn, P. Perona. Recognition in terra incognita. In *Proceedings of the European Conference on Computer Vision (ECCV)*. 2018.
- [9] Zhang, Y., H. Tan, M. Bansal. Diagnosing the environment bias in vision-and-language navigation. In C. Bessiere, ed., *Proceedings of the Twenty-Ninth International Joint Conference on Artificial Intelligence, IJCAI 2020*, pages 890–897. ijcai.org, 2020.
- [10] Pearl, J. *Causality*. Cambridge university press, 2009.
- [11] Peters, J., P. Buhlmann, N. Meinshausen. Causal inference using invariant prediction: identification and confidence intervals. *arXiv: Methodology*, 2015.
- [12] Arjovsky, M., L. Bottou, I. Gulrajani, et al. Invariant risk minimization, 2020.
- [13] Mahajan, D., S. Tople, A. Sharma. Domain generalization using causal matching. In *International Conference on Machine Learning*, pages 7313–7324. PMLR, 2021.
- [14] Liu, C., X. Sun, J. Wang, et al. Learning causal semantic representation for out-of-distribution prediction. *Advances in Neural Information Processing Systems*, 34, 2021.
- [15] Lu, C., Y. Wu, J. M. Hernández-Lobato, et al. Invariant causal representation learning for out-of-distribution generalization. In *International Conference on Learning Representations*. 2022.
- [16] Wald, Y., A. Feder, D. Greenfeld, et al. On calibration and out-of-domain generalization. In A. Beygelzimer, Y. Dauphin, P. Liang, J. W. Vaughan, eds., *Advances in Neural Information Processing Systems*. 2021.
- [17] Gulrajani, I., D. Lopez-Paz. In search of lost domain generalization. In *International Conference on Learning Representations*. 2020.
- [18] Sagawa, S., P. W. Koh, T. B. Hashimoto, et al. Distributionally robust neural networks for group shifts: On the importance of regularization for worst-case generalization. *arXiv preprint arXiv:1911.08731*, 2019.
- [19] Sun, B., K. Saenko. Deep coral: Correlation alignment for deep domain adaptation. In *European conference on computer vision*, pages 443–450. Springer, 2016.
- [20] Li, D., Y. Yang, Y.-Z. Song, et al. Deeper, broader and artier domain generalization. In *Proceedings of the IEEE international conference on computer vision*, pages 5542–5550. 2017.
- [21] Beery, S., G. Van Horn, P. Perona. Recognition in terra incognita. In *Proceedings of the European conference on computer vision (ECCV)*, pages 456–473. 2018.

- [22] Blei, D. M., A. Kucukelbir, J. D. McAuliffe. Variational inference: A review for statisticians. *Journal of the American statistical Association*, 112(518):859–877, 2017.
- [23] Sriperumbudur, B., K. Fukumizu, A. Gretton, et al. Density estimation in infinite dimensional exponential families. *Journal of Machine Learning Research*, 18(57):1–59, 2017.
- [24] Kingma, D. P., M. Welling. Auto-encoding variational bayes. *arXiv preprint arXiv:1312.6114*, 2013.
- [25] Motiian, S., M. Piccirilli, D. A. Adjeroh, et al. Unified deep supervised domain adaptation and generalization. In *Proceedings of the IEEE international conference on computer vision*, pages 5715–5725. 2017.
- [26] Dawid, A. P. Conditional independence in statistical theory. *Journal of the Royal Statistical Society. Series B (Methodological)*, 41(1):1–31, 1979.
- [27] Rosenbaum, P. R., D. B. Rubin. The central role of the propensity score in observational studies for causal effects. *Biometrika*, 70(1):41–55, 1983.
- [28] Vapnik, V. Statistical learning theory wiley. 1998.
- [29] He, K., X. Zhang, S. Ren, et al. Deep residual learning for image recognition. In *Proceedings of the IEEE conference on computer vision and pattern recognition*, pages 770–778. 2016.
- [30] Lecun, Y., L. Bottou, Y. Bengio, et al. Gradient-based learning applied to document recognition. *Proceedings of the IEEE*, 86(11):2278–2324, 1998.
- [31] Zhang, M. M., H. Marklund, N. Dhawan, et al. Adaptive risk minimization: Learning to adapt to domain shift. In A. Beygelzimer, Y. Dauphin, P. Liang, J. W. Vaughan, eds., *Advances in Neural Information Processing Systems*. 2021.
- [32] Krueger, D., E. Caballero, J.-H. Jacobsen, et al. Out-of-distribution generalization via risk extrapolation (rex). In *International Conference on Machine Learning*, pages 5815–5826. PMLR, 2021.
- [33] Bellot, A., M. van der Schaar. Accounting for unobserved confounding in domain generalization. *arXiv preprint arXiv:2007.10653*, 2020.
- [34] Kamath, P., A. Tangella, D. J. Sutherland, et al. Does invariant risk minimization capture invariance? In *AISTATS*. 2021.
- [35] Rosenfeld, E., P. Ravikumar, A. Risteski. The risks of invariant risk minimization. *arXiv preprint arXiv:2010.05761*, 2020.
- [36] Guo, R., P. Zhang, H. Liu, et al. Out-of-distribution prediction with invariant risk minimization: The limitation and an effective fix. *arXiv preprint arXiv:2101.07732*, 2021.
- [37] Makar, M., B. Packer, D. Moldovan, et al. Causally motivated shortcut removal using auxiliary labels. In G. Camps-Valls, F. J. R. Ruiz, I. Valera, eds., *Proceedings of The 25th International Conference on Artificial Intelligence and Statistics*, vol. 151 of *Proceedings of Machine Learning Research*, pages 739–766. PMLR, 2022.
- [38] Puli, A. M., L. H. Zhang, E. K. Oermann, et al. Out-of-distribution generalization in the presence of nuisance-induced spurious correlations. In *International Conference on Learning Representations*. 2022.
- [39] Khemakhem, I., D. Kingma, R. Monti, et al. Variational autoencoders and nonlinear ica: A unifying framework. In *International Conference on Artificial Intelligence and Statistics*, pages 2207–2217. PMLR, 2020.
- [40] Holland, P. W. Statistics and causal inference. *Journal of the American Statistical Association*, 81(396):945–960, 1986.
- [41] Schwab, P., L. Linhardt, W. Karlen. Perfect Match: A Simple Method for Learning Representations For Counterfactual Inference With Neural Networks. *arXiv preprint arXiv:1810.00656*, 2018.

A Proofs

In this section, we give full proofs of the main theorems in the paper.

A.1 Balanced Distribution

A.1.1 Proof for theorem 1

Here we give a proof of the minimax optimality of the Bayes optimal classifier trained on a balanced distribution.

Proof. The Bayes optimal classifier trained on a balanced distribution $p^B(X, Y)$ has $p_\psi(Y|X) = p^B(Y|X)$. Then consider the expected cross entropy loss of such classifier on an unseen test distribution p^e :

$$L^e(p^B(Y|X)) = -\mathbb{E}_{p^e(X,Y)} \log p^B(Y|X) \quad (11)$$

$$= -\mathbb{E}_{p^e(X,Y)} \log p^B(Y) + \mathbb{E}_{p^e(X,Y)} \log \frac{p^B(Y)}{p^B(Y|X)} \quad (12)$$

$$= L^e(p^B(Y)) + \mathbb{E}_{p^e(X,Y,Z)} \left[\log \frac{p^B(Y)}{p^B(Y|X)} \right] \quad (13)$$

$$= L^e(p^B(Y)) + \mathbb{E}_{p^e(Y,Z)} \left[\mathbb{E}_{p^B(X|Y,Z)} \left[\log \frac{p^B(Y)}{p^B(Y|X)} \right] \right] \quad (14)$$

$$= L^e(p^B(Y)) + \mathbb{E}_{p^e(Y,Z)} \left[\mathbb{E}_{p^B(X|Y,Z)} \left[\log \frac{p^B(Y|Z)}{p^B(Y|X, Z)} \right] \right] \quad (15)$$

$$= L^e(p^B(Y)) - \mathbb{E}_{p^e(Y,Z)} KL[p^B(Y|X, Z) || p^B(Y|Z)] \quad (16)$$

- eq. (11) is the definition of cross entropy loss.
- eq. (13) is obtained by $Y \perp\!\!\!\perp_B Z$ and $Y \perp\!\!\!\perp_B Z|X$.

Thus we have the cross entropy loss of $p^B(X, Y)$ in any environment e is smaller than that of $p^B(Y) = \frac{1}{m}$ (random guess):

$$L^e(p^B(Y|X)) - L^e(p^B(Y)) \leq -\mathbb{E}_{p^e(Y,Z)} KL[p^B(Y|X, Z) || p^B(Y|Z)] \leq 0$$

Which means:

$$\max_{e' \in \mathcal{E}} [L^{e'}(p^B(Y|X)) - L^{e'}(p^B(Y))] \leq 0$$

That is, the performance of $p^B(X, Y)$ is at least as good as random guess in any environment. Since we make an assumption of the environment diversity, that is for any p^e with $Y \not\perp\!\!\!\perp_e Z$, there exist a environment e' such that $p^e(Y|X)$ performs worse than random guess. So we have:

$$\max_{e' \in \mathcal{E}} [L^{e'}(p^B(Y|X)) - L^{e'}(p^B(Y))] \leq 0 < \max_{e' \in \mathcal{E}} [L^{e'}(p^e(Y|X)) - L^{e'}(p^B(Y))]$$

Now we want to prove that $\forall e \in \mathcal{E}, Y \perp\!\!\!\perp_e Z, Y \perp\!\!\!\perp_e Z|X, p^e(Y) = \frac{1}{m} \implies p^e(Y|X) = p^B(Y|X)$. For any $Z \in \mathcal{Z}$, we have:

$$p^e(Y|X) = p^e(Y|X, Z) = p^e(Y) \frac{p^e(X|Y, Z)}{\mathbb{E}_{p^e(Y|Z)}[p^e(X|Z, Y)]} = p^B(Y) \frac{p^B(X|Y, Z)}{\mathbb{E}_{p^B(Y)}[p^B(X|Z, Y)]} = p^B(Y|X, Z) = p^B(Y|X)$$

Thus we have the following minimax optimality:

$$p^B(Y|X) = \operatorname{argmin}_{p_\psi \in \mathcal{F}} \max_{e \in \mathcal{E}} L^e(p_\psi(Y|X))$$

□

A.2 Latent Covariate Learning

A.2.1 Proof for theorem 2

We now prove theorem 2 setting up the identifiability of the necessary parameters that capture the spuriously correlated covariate features in the VAE. The proof of this Theorem is based on the proof of Theorem 1 in [25], with the following modifications:

1. We use both E and Y as auxiliary variables.
2. We include Y in the causal mechanism of generating X by $X = \mathbf{f}(Y, Z) + \epsilon = \mathbf{f}_Y(Z) + \epsilon$.

Proof. Step I. In this step, we transform the equality of the marginal distributions over observed data into the equality of a noise-free distribution. Suppose we have two sets of parameters $\theta = (\mathbf{f}, \mathbf{T}, \lambda)$ and $\theta' = (\mathbf{f}', \mathbf{T}', \lambda')$ such that $p_\theta(X|Y, E = e) = p_{\theta'}(X|Y, E = e)$, $\forall e \in \mathcal{E}_{\text{train}}$, then:

$$\int_{\mathcal{Z}} p_{\mathbf{T}, \lambda}(Z|Y, E = e) p_{\mathbf{f}}(X|Z, Y) dZ = \int_{\mathcal{Z}} P_{\mathbf{T}', \lambda'}(Z|Y, E = e) p'_{\mathbf{f}}(X|Z, Y) dZ \quad (17)$$

$$\Rightarrow \int_{\mathcal{Z}} p_{\mathbf{T}, \lambda}(Z|Y, E = e) p_{\epsilon}(X - \mathbf{f}_Y(Z)) dZ = \int_{\mathcal{Z}} p_{\mathbf{T}', \lambda'}(Z|Y, E = e) p_{\epsilon}(X - \mathbf{f}'_Y(Z)) dZ \quad (18)$$

$$\Rightarrow \int_{\mathcal{X}} p_{\mathbf{T}, \lambda}(\mathbf{f}^{-1}(\bar{X})|Y, E = e) \text{vol} J_{\mathbf{f}^{-1}}(\bar{X}) p_{\epsilon}(X - \bar{X}) d\bar{X} = \int_{\mathcal{X}} p_{\mathbf{T}', \lambda'}(\mathbf{f}'^{-1}(\bar{X})|Y, E = e) \text{vol} J_{\mathbf{f}'^{-1}}(\bar{X}) p_{\epsilon}(X - \bar{X}) d\bar{X} \quad (19)$$

$$\Rightarrow \int_{\mathbb{R}^d} \tilde{p}_{\mathbf{T}, \lambda, \mathbf{f}, Y, e}(\bar{X}) p_{\epsilon}(X - \bar{X}) d\bar{X} = \int_{\mathbb{R}^d} \tilde{p}_{\mathbf{T}', \lambda', \mathbf{f}', Y, e}(\bar{X}) p_{\epsilon}(X - \bar{X}) d\bar{X} \quad (20)$$

$$\Rightarrow (\tilde{p}_{\mathbf{T}, \lambda, \mathbf{f}, Y, e} * p_{\epsilon})(X) = (\tilde{p}_{\mathbf{T}', \lambda', \mathbf{f}', Y, e} * P_{\epsilon})(X) \quad (21)$$

$$\Rightarrow \mathcal{F}[\tilde{p}_{\mathbf{T}, \lambda, \mathbf{f}, Y, e}](\omega) \phi_{\epsilon}(\omega) = \mathcal{F}[\tilde{p}_{\mathbf{T}', \lambda', \mathbf{f}', Y, e}](\omega) \phi_{\epsilon}(\omega) \quad (22)$$

$$\Rightarrow \mathcal{F}[\tilde{p}_{\mathbf{T}, \lambda, \mathbf{f}, Y, e}](\omega) = \mathcal{F}[\tilde{p}_{\mathbf{T}', \lambda', \mathbf{f}', Y, e}](\omega) \quad (23)$$

$$\Rightarrow \tilde{p}_{\mathbf{T}, \lambda, \mathbf{f}, Y, e}(X) = \tilde{p}_{\mathbf{T}', \lambda', \mathbf{f}', Y, e}(X) \quad (24)$$

- In eq. (19), we denote the volume of a matrix \mathbf{A} as $\text{vol} \mathbf{A} := \sqrt{\det \mathbf{A}^T \mathbf{A}}$. J denotes the Jacobian. We made the change of variable $\bar{X} = \mathbf{f}_Y(Z)$ on the left hand side and $\bar{X} = \mathbf{f}'_Y(Z)$ on the right hand side. Since \mathbf{f} is injective, we have $\mathbf{f}^{-1}(\bar{X}) = (Y, Z)$. Here we abuse $\mathbf{f}^{-1}(\bar{X})$ to specifically denote the recovery of Z , i.e. $\mathbf{f}^{-1}(\bar{X}) = Z$.

- In eq. (20), we introduce

$$\tilde{p}_{\mathbf{T}, \lambda, \mathbf{f}, Y, e}(X) = p_{\mathbf{T}, \lambda}(\mathbf{f}_Y^{-1}(X)|Y, E = e) \text{vol} J_{\mathbf{f}_Y^{-1}}(X) \mathbb{1}_{\mathcal{X}}(X) \quad (25)$$

on the left hand side, and similarly on the right hand side.

- In eq. (21), we use $*$ for the convolution operator.
- In eq. (22), we use $\mathcal{F}[\cdot]$ to designate the Fourier transform, and the characteristic function of ϵ is $\phi_{\epsilon} = \mathcal{F}[p_{\epsilon}]$.
- In eq. (23), we dropped $\phi_{\epsilon}(\omega)$ from both sides as it is non-zero almost everywhere (by assumption (1) of the Theorem).

Step II. In this step, we remove all terms that are either a function of X or Y or e . By taking logarithm on both sides of eq. (24) and replacing $P_{\mathbf{T}, \lambda}$ by its expression from Equation (3) we get:

$$\begin{aligned} & \log \text{vol} J_{\mathbf{f}^{-1}}(X) + \sum_{i=1}^n (\log Q_i(\mathbf{f}_i^{-1}(X))) - \log W_i^e(Y) + \sum_{j=1}^k \mathbf{T}_{i,j}(\mathbf{f}_i^{-1}(X)) \lambda_{i,j}^e(Y) \\ &= \log \text{vol} J_{\mathbf{f}'^{-1}}(X) + \sum_{i=1}^n (\log Q'_i(\mathbf{f}'_i^{-1}(X))) - \log W_i'^e(Y) + \sum_{j=1}^k \mathbf{T}'_{i,j}(\mathbf{f}'_i^{-1}(X)) \lambda'_{i,j}(Y) \end{aligned} \quad (26)$$

Let $(e_0, y_0), (e_1, y_1), \dots, (e_{nk}, y_{nk})$ be the points provided by assumption (3) of the Theorem. We evaluate the above equations at these points to obtain $k + 1$ equations, and subtract the first equation from the remaining k equations to obtain:

$$\begin{aligned} & \langle \mathbf{T}(\mathbf{f}^{-1}(X)), \lambda^{e_l}(y_l) - \lambda^{e_0}(y_0) \rangle + \sum_{i=1}^n \log \frac{W_i^{e_0}(y_0)}{W_i^{e_l}(y_l)} \\ &= \langle \mathbf{T}'(\mathbf{f}^{-1}(X)), \lambda^{e_l}(y_l) - \lambda^{e_0}(y_0) \rangle + \sum_{i=1}^n \log \frac{W_i'^{e_0}(y_0)}{W_i'^{e_l}(y_l)} \end{aligned} \quad (27)$$

Let \mathbf{L} be the matrix defined in assumption (3) and \mathbf{L}' similarly defined for λ' (\mathbf{L}' is not necessarily invertible). Define $b_l = \sum_{i=1}^n \log \frac{W_i'^{e_0}(y_0) W_i^{e_l}(y_l)}{W_i^{e_0}(y_0) W_i'^{e_l}(y_l)}$ and $\mathbf{b} = [b_l]_{l=1}^{nk}$.

Then eq. (27) can be rewritten in the matrix form:

$$\mathbf{L}^T \mathbf{T}(\mathbf{f}^{-1}(X)) = \mathbf{L}'^T \mathbf{T}'(\mathbf{f}'^{-1}(X)) + \mathbf{b} \quad (28)$$

We multiply both sides of eq. (28) by \mathbf{L}^{-T} to get:

$$\mathbf{T}(\mathbf{f}^{-1}(X)) = \mathbf{A} \mathbf{T}'(\mathbf{f}'^{-1}(X)) + \mathbf{c} \quad (29)$$

Where $\mathbf{A} = \mathbf{L}^{-T} \mathbf{L}'$ and $\mathbf{c} = \mathbf{L}^{-T} \mathbf{b}$.

Step III. To complete the proof, we need to show that \mathbf{A} is invertible. By definition of \mathbf{T} and according to Assumption (2), its Jacobian exists and is an $nk \times n$ matrix of rank n . This implies that the Jacobian of $\mathbf{T}' \circ \mathbf{f}'^{-1}$ exists and is of rank n and so is \mathbf{A} .

We distinguish two cases:

1. If $k = 1$, then \mathbf{A} is invertible as $\mathbf{A} \in \mathbb{R}^{n \times n}$.
2. If $k > 1$, define $\bar{\mathbf{x}} = \mathbf{f}^{-1}(\mathbf{x})$ and $\mathbf{T}_i(\bar{x}_i) = (T_{i,1}(\bar{x}_i), \dots, T_{i,k}(\bar{x}_i))$.

Suppose for any choice of $\bar{x}_i^1, \bar{x}_i^2, \dots, \bar{x}_i^k$, the family $(\frac{d\mathbf{T}_i(\bar{x}_i^1)}{d\bar{x}_i^1}, \dots, \frac{d\mathbf{T}_i(\bar{x}_i^k)}{d\bar{x}_i^k})$ is never linearly independent. This means that $\mathbf{T}_i(\mathbb{R})$ is included in a subspace of \mathbb{R}^k of dimension of most $k - 1$. Let \mathbf{h} be a non-zero vector that is orthogonal to $T_i(\mathbb{R})$. Then for all $x \in \mathbb{R}$, we have $\langle \frac{d\mathbf{T}_i(x)}{dx}, \mathbf{h} \rangle = 0$. By integrating we find that $\langle \mathbf{T}_i(x), \mathbf{h} \rangle = \text{const}$.

Since this is true for all $x \in \mathbb{R}$ and for a $h \neq 0$, we conclude that the distribution is not strongly exponential. So by contradiction, we conclude that there exist k points $\bar{x}_i^1, \bar{x}_i^2, \dots, \bar{x}_i^k$ such that $(\frac{d\mathbf{T}_i(\bar{x}_i^1)}{d\bar{x}_i^1}, \dots, \frac{d\mathbf{T}_i(\bar{x}_i^k)}{d\bar{x}_i^k})$ are linearly independent.

Collect these points into k vectors $(\bar{\mathbf{x}}^1, \dots, \bar{\mathbf{x}}^k)$ and concatenate the k Jacobians $J_{\mathbf{T}}(\bar{\mathbf{x}}^l)$ evaluated at each of those vectors horizontally into the matrix $\mathbf{Q} = (J_{\mathbf{T}}(\bar{\mathbf{x}}^1), \dots, J_{\mathbf{T}}(\bar{\mathbf{x}}^k))$ and similarly define \mathbf{Q}' as the concatenation of the Jacobians of $\mathbf{T}'(\mathbf{f}'^{-1} \circ \mathbf{f}(\bar{\mathbf{x}}))$ evaluated at those points. Then the matrix \mathbf{Q} is invertible. By differentiating eq. (29) for each \mathbf{x}^l , we get:

$$\mathbf{Q} = \mathbf{A} \mathbf{Q}' \quad (30)$$

The invertibility of \mathbf{Q} implies the invertibility of \mathbf{A} and \mathbf{Q}' . This completes the proof. \square

A.3 Balanced mini-batch sampling

A.3.1 Proof for theorem 3

Our proof of all possible balancing scores is an extension of the proof of Theorem 2 from [27], by generalizing the binary treatment to multiple treatments.

Proof. First, suppose the balancing score $b(Z)$ is finer than the propensity score $s(Z)$. By the definition of a balancing score (definition 3) and Bayes' rule, we have:

$$p(Y|Z, b(Z)) = p(Y|b(Z)) \quad (31)$$

On the other hand, since $b(Z)$ is a function of Z , we have:

$$p(Y|Z, b(Z)) = p(Y|Z) \quad (32)$$

eq. (31) and eq. (32) give us $p(Y|b(Z)) = p(Y|Z)$. So to show $b(Z)$ is a balancing score, it is sufficient to show $p(Y|b(Z)) = p(Y|Z)$.

Let the y -th entry of $S(Z)$ be $s_y(Z) = p(Y = y|Z)$, then:

$$\mathbb{E}[s_y(Z)|b(Z)] = \int_{\mathcal{Z}} p(Y = y|Z = z)p(Z = z|b(Z))dz = p(Y = y|b(Z)) \quad (33)$$

But since $b(Z)$ is finer than $s(Z)$, $b(Z)$ is also finer than $s_y(Z)$, then

$$\mathbb{E}[s_y(Z)|b(Z)] = s_y(Z) \quad (34)$$

Then by eq. (33) and eq. (34) we have $P(Y = y|Z) = P(Y = y|b(Z))$ as required. So $b(Z)$ is a balancing score.

For the converse, suppose $b(Z)$ is a balancing score, but that $b(Z)$ is not finer than $s(Z)$. Then there exists z_1 and z_2 such that $s(z_1) \neq s(z_2)$, but $b(z_1) = b(z_2)$. By the definition of $s(\cdot)$, there exists y such that $P(Y = y|z_1) \neq P(Y = y|z_2)$. This means, Y and Z are not conditionally independent given $b(Z)$, thus $b(Z)$ is not a balancing score. Therefore, to be a balancing score, $b(Z)$ must be finer than $s(Z)$.

Note that $s(Z)$ is also a balancing score, since $s(Z)$ is also a function of itself.

□

A.3.2 Proof for theorem 4

We provide a proof for theorem 4, demonstrating the feasibility of balanced mini-batch sampling.

Proof. In algorithm 1, by uniformly sampling a different labels such that $y \neq y^e$, we mean sample $Y_{\text{alt}} = \{y_1, y_2, \dots, y_a\}$ by the following procedure:

$$\begin{aligned} y_1 &\sim U\{1, 2, \dots, m\} \setminus \{y_e\} \\ y_2 &\sim U\{1, 2, \dots, m\} \setminus \{y_e, y_1\} \\ &\vdots \\ y_a &\sim U\{1, 2, \dots, m\} \setminus \{y_e, y_1, y_2, \dots, y_{a-1}\} \end{aligned}$$

Where U denotes the uniform distribution. Suppose $D_{\text{balanced}} \sim \hat{p}^B(X, Y)$, and data distribution $\mathcal{D}^e \sim p(X, Y|E = e), \forall e \in \mathcal{E}_{\text{train}}$.

Suppose we have an exact match every time we match a balancing score, then for all $e \in \mathcal{E}_{\text{train}}$, we have

$$\begin{aligned}
\hat{p}^B(Y|b^e(Z), E=e) &= \frac{1}{a+1}p(Y|b^e(Z), E=e) + \frac{1}{a+1}(1-p(Y|b^e(Z), E=e))\frac{1}{m-1} + \\
&+ \frac{1}{a+1}(1-p(Y|b^e(Z), E=e))(1-\frac{1}{m-1})\frac{1}{m-2} + \dots \\
&+ \frac{1}{a+1}(1-p(Y|b^e(Z), E=e))(1-\frac{1}{m-1})(1-\frac{1}{m-2})\dots(1-\frac{1}{m-a+1})\frac{1}{m-a} \\
&= \frac{1}{a+1}(\frac{a}{m-1} + \frac{m-a-1}{m-1}p(Y|b^e(Z), E=e))
\end{aligned}$$

By the definition of balancing score, $p(Y|Z, E=e) = p(Y|b^e(Z), E=e)$ and $\hat{p}^B(Y|Z, E=e) = \hat{p}^B(Y|b^e(Z), E=e)$, then we have

$$\hat{p}^B(Y|Z, E) = \frac{1}{a+1}(\frac{a}{m-1} + \frac{m-a-1}{m-1}p(Y|Z, E)) \quad (35)$$

When $a = m - 1$, we have $\hat{p}^B(Y|Z, E) = \frac{1}{m} = U\{1, 2, \dots, m\}$, which means $\hat{p}^B(X, Y, Z) = p^B(X, Y, Z)$. i.e. D_{balanced} can be regarded as sampled from the balanced distribution p^B as defined in definition 1. □

B Experiment Details

All experiments were conducted on NVidia A-100 and Titan X GPUs. The DomainBed codebase is released under an MIT license at <https://github.com/facebookresearch/DomainBed>. We utilize versions of the datasets ColoredMNIST, PACS, and TerraIncognita (Caltech Camera Traps) that are distributed within DomainBed, under the Creative Commons Attribution-NonCommercial 4.0, Copy-Left/No Rights Reserved, and Community Data License Agreement (CDLA) licenses respectively. Our code and corresponding instructions are included in the supplementary materials.

The “optimal” hyperparameters were extracted from their full experimental logs provided at <https://drive.google.com/file/d/16VFQWTble6-nB5AdXBtQpQFwjEC7CChM/>. To retrieve hyperparameters, we ran the script `list_top_hparams.py` and collected the top two highest-performant hyperparameter dicts and experiment seeds for each (dataset, model, environment) pair in our results table. We completed train/test runs to convergence for each combination of (top model, seed) for the trial seeds in (0,1,2) in each condition. From these results we ran the `collect_results.py` script to gather the results reported in the above tables.

Table 3: Out-of-domain test accuracy on each domain of the PACS dataset. Numbers are averaged over 3 runs. We use Gaussian distribution with $k = 2$ for latent covariate learning and $n = 64$.

	Sampling	Algorithm	A	C	P	S	Avg
Default hyperparameters	Random	ERM	85.0 \pm 1.6	77.9 \pm 2.2	95.4 \pm 0.3	76.4 \pm 1.1	83.7 \pm 0.1
		IRM	81.4 \pm 0.7	76.4 \pm 1.3	96.6 \pm 0.5	70.5 \pm 2.0	81.2 \pm 0.4
		GroupDRO	83.6 \pm 0.8	79.9 \pm 1.2	96.4 \pm 0.4	74.9 \pm 0.3	83.7 \pm 0.4
		CORAL	86.0 \pm 0.6	77.6 \pm 0.3	95.7 \pm 0.1	80.1 \pm 0.1	84.8 \pm 0.2
	Balanced $b(Z) = Z$	ERM	85.7 \pm 0.7	80.2 \pm 0.3	96.4 \pm 0.2	78.5 \pm 2.2	85.2 \pm 0.3
		IRM	83.6 \pm 1.2	74.7 \pm 2.0	96.6 \pm 0.3	75.6 \pm 1.6	82.6 \pm 0.3
		GroupDRO	83.6 \pm 1.2	80.1 \pm 1.2	95.1 \pm 0.5	80.2 \pm 1.3	84.7 \pm 0.6
		CORAL	82.2 \pm 1.9	79.0 \pm 1.1	96.2 \pm 0.1	79.7 \pm 0.8	84.3 \pm 0.5
	Balanced $b(Z) = s^e(Z)$	ERM	84.3 \pm 0.5	79.8 \pm 1.0	95.7 \pm 0.4	80.9 \pm 1.2	85.2 \pm 0.4
		IRM	84.2 \pm 1.7	73.8 \pm 0.7	97.1 \pm 0.4	73.4 \pm 1.2	82.1 \pm 0.6
		GroupDRO	82.7 \pm 0.9	79.0 \pm 0.9	95.5 \pm 0.3	80.0 \pm 1.3	84.3 \pm 0.4
		CORAL	84.0 \pm 1.8	81.6 \pm 0.9	94.2 \pm 0.9	80.4 \pm 1.1	85.1 \pm 0.4

Table 4: Out-of-domain test accuracy on on each domain of the TerraIncognita dataset. Numbers are averaged over 3 runs. We use Gaussian distribution with $k = 2$ for latent covariate learning and $n = 29$.

		Sampling	Algorithm	L100	L38	L43	L46	Avg
Default hyperparameters	Random		ERM	50.6 ± 4.1	42.9 ± 2.6	55.8 ± 0.1	35.1 ± 2.0	46.1 ± 1.2
			IRM	34.0 ± 4.3	33.2 ± 9.1	50.4 ± 0.8	9.6 ± 1.1	39.3 ± 1.8
			GroupDRO	50.0 ± 1.9	36.5 ± 4.8	56.3 ± 0.8	31.7 ± 3.1	43.6 ± 1.2
			CORAL	48.5 ± 2.9	37.9 ± 4.0	55.5 ± 2.1	37.3 ± 0.9	44.8 ± 0.3
	Balanced $b(Z) = Z$		ERM	50.5 ± 2.9	45.1 ± 1.1	55.6 ± 0.9	37.4 ± 1.0	47.1 ± 0.6
			IRM	32.0 ± 3.9	40.8 ± 2.9	49.0 ± 1.5	38.7 ± 1.3	40.1 ± 1.4
			GroupDRO	48.7 ± 3.1	23.3 ± 4.2	55.7 ± 1.0	38.5 ± 1.4	41.6 ± 1.5
			CORAL	54.9 ± 2.8	41.3 ± 0.9	55.2 ± 0.7	37.7 ± 1.7	47.3 ± 0.4
	Balanced $b(Z) = s^e(Z)$		ERM	51.9 ± 0.4	45.8 ± 2.4	55.0 ± 1.0	39.8 ± 1.3	48.1 ± 0.3
			IRM	37.6 ± 7.2	43.0 ± 1.8	43.5 ± 3.8	36.9 ± 1.8	40.2 ± 2.9
			GroupDRO	49.7 ± 2.7	34.6 ± 2.5	54.5 ± 1.2	33.4 ± 2.7	43.1 ± 0.6
			CORAL	50.1 ± 2.1	42.6 ± 2.1	54.7 ± 0.8	37.3 ± 2.5	46.2 ± 0.4

C Broader Impact

Techniques for provably reducing the influence of spurious correlations on classification problems could be a boon for the reliability of and trust in general public-facing AI systems. Considering that these spurious correlations are present across a wide array of datasets and tasks, the balanced mini-batch sampling techniques we propose herein could be broadly applicable for general system reliability improvements in supervised learning settings, without modification of the classification model.

As for risks, we estimate that our proposed methods are not particularly rife for abuse, and pose a low level of danger broadly comparable to other innovations in optimizers, loss functions, and neural network architectures. We believe there is not a significant risk of any code or data produced for this study being used to nefarious ends.